Two-dimensional first-order phase transition as signature change event in contact statistical manifolds with Finsler metric

V. Balan, H. Grushevskaya, N. Krylova, G. Krylov and I. Lipnevich

Abstract. In this work we propose a phase transition model associated with the metric–signature–change events in its pseudo-Finsler–Langmuir configuration space. We prove that the change of signature of the contact statistical manifold endowed with a Langmuir–Finsler metric occurs, and that this event corresponds to the first-order phase transition in the Langmuir monolayer under compression. We determine the Cartan tensor and the nonlinear Barthel connection, which provide a tool to estimate how far is the Finsler model from the pseudo-Euclidean one, and to construct the Finsler adapted frames for the module of sections of the tangent bundle. As well, the Berwald curvature of the Finsler space is explicitly determined and it is shown that it vanishes everywhere except the regions of anomaly which correspond to the phase transition.

1   Introduction

High-ordered graphene-like nanostructures may exhibit unique electro-physical and optical properties [1, 2]. A type of such structures is presented by the Langmuir – Blodgett (LB) films, which are formed at air/liquid interface, under the compression of a Langmuir monomolecular layer (monolayer) of amphiphilic molecules [3, 4, 5] with a subsequent deposition on the substrate. The properties of the LB-film vary in dependence on the compression parameters, namely, the compression rate, the subphase acidity, and the temperature [6]. Because of this, the issue of theoretical modeling the Langmuir monolayer is a crucial issue in nanothechnology. Of particular interest is the description of the two-dimensional first-order liquid-crystalline phase transition in the monolayers [7, 8, 9, 10].

1.1 Riemannian geometrization of the phase transition thermodynamics

It is known [11, 12] that the necessary condition for phase stability is the positiveness of the Hessian of the Gibbs free energy in the expansion of the energy increment over the thermodynamic variables. With such an approach one can introduce a metric for the space of thermodynamic variables, and further use Riemann geometry methods [13, 14]. The scalar curvature in such a geometrization of the thermodynamics can be expressed in terms of such matter thermodynamic quantities, as compressibility κ, thermal expansion, and heat capacity. It is cornerstone that the priority of such approach is the analysis of a geometric characteristic tensor – the curvature, regarded as generalized thermodynamic parameter, instead of considering a large number of thermodynamic inequalities. The heat capacity and compressibility undergo the divergence at phase transitions. During the phase transition, the divergence of the thermodynamic quantities are expected to imply the divergence of the other parameters, including the curvature. However, for well-known Ruppeiner's [15] and Weinhold's [13, 14] metrics the scalar curvature remains finite at a critical point, when one of the above mentioned thermodynamic quantities tends to infinity, while the rest remain fixed [16]. In [17], the thermodynamics was geometrized with a metric, whose scalar curvature diverges at the critical point. The Quevedo's metric satisfactorily describes second-order phase transitions without metastable states [16]. The physical nature of the first order phase transition at a triple point is similar to the second order phase transition [18]. But, in contrast to the second order phase transitions, κ and other matter thermodynamic quantities exhibit a change of sign in the vicinity of the 1st-order phase transition. In [16] a metric on the thermodynamic variables space was proposed. A scalar curvature of the thermodynamic space diverges and differs by sign for stable and metastable states at the critical point. Unfortunately, this metric is not invariant with respect to the Legendre transformation. Therefore, nowadays, the problem of appropriate geometrization of thermodynamics to describe the first order phase transition is still actual.

1.2 Geometry of systems with constrains

A Finsler geometrization of electro-capillary interactions in Langmuir monolayers was proposed in [19, 20]. An action S of the contact Finsler–Lagrangian statistical manifold describes the entropy of two-dimensional (2D) monolayer. This pseudo-Finsler space can possess the specific feature that a part of the tangent vectors lie on the hypercone which is similar to the light cones from Relativity Theory ([21, 22]). The Finsler structure lives on the associated geometric vector bundle over the slit tangent space, which infers that the fundamental Finsler function (pseudonorm) may be considered as an action for a physical system. A Finsler function of the monolayer provides a large number of indicatrix classes. However, the link between these solutions and the real observed monolayer structures was not completely clarified yet.

Phase transitions associated with the events which accompany the change in metric signature (for example, the transition between the $(+\ -\ -\ -)$ and $(+\ +\ -\ -)$ space–time signatures), are considered in cosmological models of loop quantum gravity [23, 24] and their analogues, the signature change events in Bose gas hydrodynamics [25], and in optical metamaterials [26]. In such phase transitions, both the total

number and the total energy of the particles generated in a signature change event are formally infinite. Due to this fact, such a transition, for example, is called in cosmology "a big flash", and shares certain similarities with the cosmological "big bang". Opposite to usual phase transitions, in which the physical system changes while the background metric is considered intact, the signature change transition affects the underlying background metric experienced by the system.

The 2D phase transitions of first order in compressed Langmuir monolayers, depart from the 3D first-order phase transitions, are accompanied by the occurrence of visualizing fractal-like structures in a region where liquid and crystal phases coexist [27, 28]. In such regions dependencies of the surface pressure π upon the area A per molecule (compression $\pi - A$-isotherm) can have a plateau that is a curve piece with small slope. The slope of the plateau for the 2D 1st-order phase transition depends on the compression speed, while the plateau of isotherms for 3D 1st-order phase transitions is horizontal. The character of the compressibility of the monolayer depends as well on the compression speed. In the paper we will show that modeling the 2D first-order phase transition in the 3D contact statistical manifold as a metric signature change event in the corresponding Finsler space allows us explain these features of the 1st-order phase transitions in monolayers.

Our main goal is to study first-order phase transitions in Langmuir monolayers as signature change events in the configuration pseudo-Finsler space. Our finding is that a Langmuir monolayer self-organization occurs, when the Berwald scalar curvature of Finsler space behaves in an anomalous manner. We predict three types of monolayer self-organization. The first two types are structurization in isotropic and anisotropic fields of velocities. The third type is a glass-like state, in which there coexist regions of finite and infinite motions. We show that the particles of the monolayer describe closed paths with the limit cycle similar to a strange attractor of relaxation oscillations. However, they still may drift to non-closed trajectories, since the regions of finite and infinite motions are separated only by punctured neighborhood within the space of velocities.

2   Riemann–Finsler structures in monolayer structurization

The hydrated molecules in the Langmuir monolayer are located on the boundary between air and aqueous medium. During the compression process, the molecules are extruded from the hydration shells. Meanwhile, the molecules extruded from the water interact with each other and form the Langmuir–Blodgett monolayer film. An entropy dynamics of particles changing their masses is described by the pseudo-Finsler metric function. In the entropy representation the metric function, which describes the phase-transition dynamics of the radially-symmetric compressed monolayer with polar coordinates r, ϕ on the contact statistical manifold, has been constructed in [20], and has the following form:

$$(2.1) \qquad L = \left[A\frac{\dot{\xi}}{\dot{r}} + B \right] \left\{ \dot{\xi}^2 - \frac{C}{2} \left[A\left(\frac{\partial r}{\partial t}\right)^{-1} + B \right]^{-1} (\dot{r}^2 + r^2\dot{\phi}^2) \right\},$$

where the parameters A, B, C are given by
(2.2)
$$A = p\,|V|\,r^5 e^{\frac{2|V|t}{r}},$$

$$B = mc^2 - p\left(\left(-\tfrac{4}{3}r^5 + \tfrac{16}{15}(|V|t)r^4 + \tfrac{1}{30}(|V|t)^2 r^3 + \tfrac{1}{45}(|V|t)^3 r^2 + \tfrac{1}{45}(|V|t)^4 r\right.\right.$$

$$\left.\left.+\tfrac{2}{45}(|V|t)^5\right)\,e^{\frac{2|V|t}{r}} - \tfrac{4}{45}\frac{(|V|t)^6}{r}\,\mathrm{Ei}\left[\tfrac{2|V|t}{r}\right]\right),$$

$$C = m, \quad \text{where } p = \tfrac{\pi^2 q^2}{\varepsilon\varepsilon_0}\,\tfrac{\rho_0^2}{R_0^2}, \quad \dot{r} = \tfrac{x\dot{x}+y\dot{y}}{r}.$$

Here $\mathrm{Ei}\left[\tfrac{2|V|t}{r}\right]$ is the special function *exponential integral*, m is the proper particle mass, V is the monolayer compression rate, p includes characteristics of the monolayer, such as molecular charge q, initial surface density ρ_0 of the molecules, and initial monolayer radius R_0. The pseudo-time t is the time of phase transition, whose flow is defined by the distribution of times of relaxation processes in the monolayer. Also, $\dot{\xi}$, $\dot{r}$ and $\dot{\varphi}$ define the corresponding derivatives of t, r and φ with respect to the evolution parameter s. The factor $C\left[A\left(\tfrac{\partial r}{\partial t}\right)^{-1} + B\right]^{-1}$ in the expression (2.1) shows that the mass of the hydrated monolayer is variable.

We also remark that (M, L) is a Lagrange space [29] which, due to the homogeneity of L, generates on different regions of the coordinate space M, corresponding Finsler structures.

2.1   Indicatrices of the monolayer-associated Finsler space

The indicatrix I_{x_0} at a point $\{x_0^i\} \in M$ is a hypersurface in $T_{x_0}M$ [22] and is defined via $F(x_0^i, y^i) = 1$, similar to a space unit sphere in the positive definite subcase, and has a definite meaning in physically feasible systems. For example, for the Zermelo navigation problem, the indicatrix consists of all the destination points which are reachable in one unit of time, while the motion is affected by a given vector field (the "wind") [30].

For the pseudo-Finsler metric we can define the "timelike" (pseudo-time) and "spacelike" indicatrices by analogy with General Relativity Theory, as

(2.3)
$$L(x_0^i, y^i) = 1$$

and

(2.4)
$$L(x_0^i, y^i) = -1$$

respectively. Fig. 1 illustrates a simulation of "timelike" and "spacelike" indicatrices, depending on the metric parameter B. According to the explicit form of the Finsler function (2.1), when the speed V of the monolayer compression tends to zero, the coefficient A tends to zero as well, and the Finsler function degenerates into pseudo-Riemannian one. The same situation occurs for enough large values of B, when the indicatrix has the form of a double- or one-sheeted hyperboloid, as shown in Fig. 1a, e. In this case, the amplitude of the particle velocities are restricted, while a velocity-direction distribution is isotropic one due to the axial symmetry of the indicatrix. But at non-zero A, there exist values of the parameter B, for which the form of the

spacetime indicatrix dramatically changes as Figs. 1i–k show. As B decreases to 10^{-15} or becomes negative (e.g., $B = -0.1$, -1), the particle velocities are restricted both in amplitude and direction. From the physical point of view, free particles transit into bounded state.
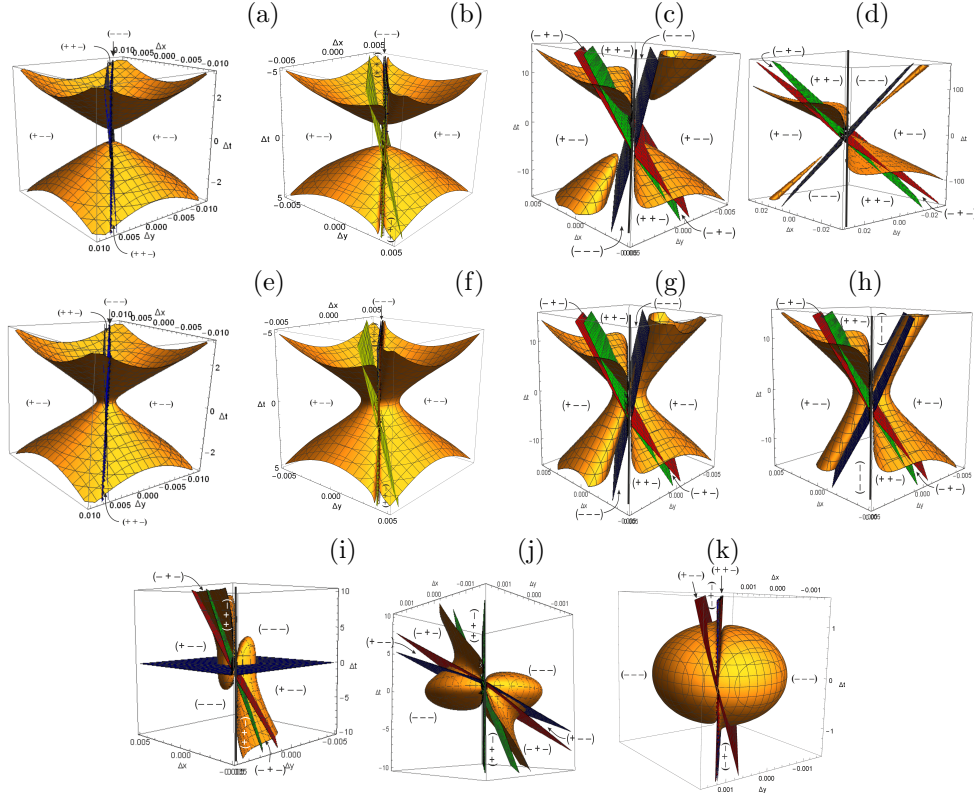

Figure 1: Indicatrices of Langmuir–Finsler space at $A = 10^{-5}$, $C = 10^6$, $r = 1$ and different B: timelike indicatrices at $B = 10$ (a), 1 (b), 0.1 (c), 0.07 (d); and space-like indicatrices of Finsler space at $B = 10$ (e), 1 (f), 0.1 (g), 0.07(h), 10^{-15} (i), -0.1 (j), -1 (k). The colored (red, blue, green and black) planes divide the $(\Delta t, \Delta x, \Delta y)$ space into the regions with the different signature denoted in brackets.

The metric tensor is defined by

$$(2.5) \qquad g_{ij} = \frac{1}{2} \frac{\partial^2 L}{\partial y^i \partial y^j}.$$

Let us investigate now the signature of the metric tensor g_{ij}. The matrix associated

to the metric tensor g_{ij} is:

$$(2.6) \qquad g_{ij} = \begin{pmatrix} 3A\dfrac{\dot{\xi}}{\dot{r}} + B & -\dfrac{3}{2}A\left(\dfrac{\dot{\xi}}{\dot{r}}\right)^2 & 0 \\[2ex] -\dfrac{3}{2}A\left(\dfrac{\dot{\xi}}{\dot{r}}\right)^2 & A\left(\dfrac{\dot{\xi}}{\dot{r}}\right)^3 - \dfrac{C}{2} & 0 \\[2ex] 0 & 0 & -\dfrac{C}{2}r^2 \end{pmatrix},$$

and hence the Jacobi minors, which are represented in Fig. 2, are:

$$\begin{cases} \Delta_1 &= 3A\dfrac{\dot{\xi}}{\dot{r}} + B, \\[2ex] \Delta_2 &= \dfrac{3A^2}{4}\left(\dfrac{\dot{\xi}}{\dot{r}}\right)^4 + AB\left(\dfrac{\dot{\xi}}{\dot{r}}\right)^3 - \dfrac{3AC}{2}\dfrac{\dot{\xi}}{\dot{r}} - \dfrac{BC}{2}, \\[2ex] \Delta_3 &= -\dfrac{C}{2}r^2\Delta_2. \end{cases}$$

The thermodynamic stability in the free energy representation requires that the Hessian is a positive-definite symmetric $(0,2)$-tensor field. Accordingly, the minimal value of the free energy requires by the positiveness of the leading principal minors ($\Delta_k > 0$). In the entropy representation, a system is thermodynamically stable if it satisfies the Second Law of Thermodynamics, namely, the entropy of the system reaches its maximum. Therefore, the indicatrices related to stable physical systems correspond to negative definite Hessians of Finsler-type Lagrangians (2.1). We further fix the following set of parameters $A = 10^{-5}$, $B = 0.12$, 0.1, 0.07, 10^{-15}, -0.07, -0.1, -0.12, $C = 10^{6}$ in Fig. 2. For all the values of B, there exist physical regions of the Finsler space where the minors determine the Hessian signature $(n_+, n_-) = (0,3)$, according to Fig. 2. Here the momentum index n_+, n_- is the number of positive and negative signs respectively in the Hessian quadratic form. For example, at $B = 10^{-15}$ one identifies the following regions for the minors Δ_1, Δ_2, Δ_3 denoted by a yellow line. In the first region, the minors are $\Delta_1 < 0$, $\Delta_2 > 0$, $\Delta_3 < 0$, leading to a negative definite Hessian quadratic form, with the signature $(0,3)$. In region 2 ($\Delta_1 > 0$, $\Delta_2 > 0$, $\Delta_3 < 0$), we have a indefinite metric with Hessian signature $(2,1)$. Finally, in region 3 ($\Delta_1 > 0$, $\Delta_2 < 0$, $\Delta_3 > 0$), we have an indefinite metric with Hessian signature $(1,2)$.

If the Hessian matrix is negative definite ($\Delta_1 < 0, \Delta_2 > 0, \Delta_3 < 0$), then the entropy is maximized. Hence, by virtue of the 2-nd law of thermodynamics, the trajectories are stable for the Finsler metrics with the Hessian signature $(0,3)$, and, respectively, the configurations of nuclei (phase elements) space become physical ones (nuclei physically exist) and are stable.

We shall further find and discuss the indicatrix pieces related to the negative definite signature. In order to discard the non-physical configurations, we shall construct the surfaces S_i, $i = 1, 2, 3$ which split the Finsler space into regions with metric constant signature.
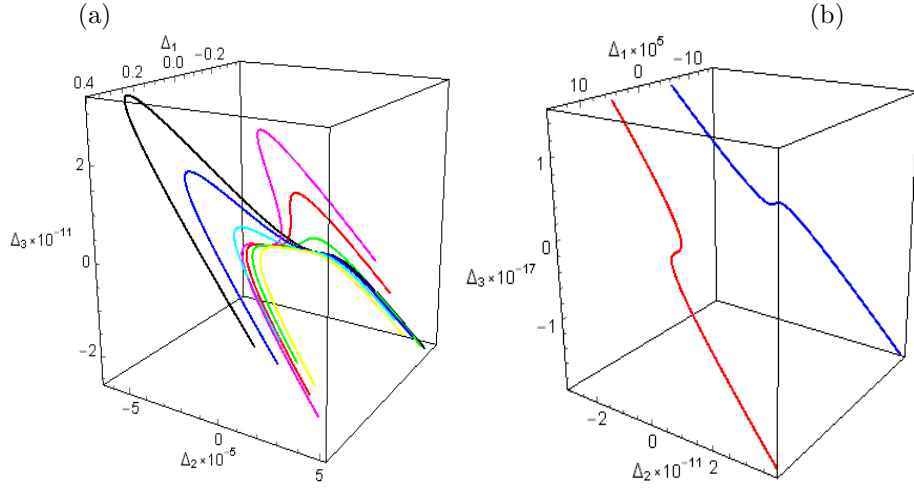
Figure 2: Behavior of the leading principal minors Δ_k, $k = 1, 2, 3$ for the Finsler-metric parameters $A = 10^{-5}$, $C = 10^6$, $r = 1$; (a) $B = 0.12$ (magenta), 0.1 (red), 0.07 (green), 10^{-15} (yellow), -0.07 (light blue), -0.1 (blue), -0.12 (black); (b) $B = 1$ (red), -1 (blue).

2.2 The metric signature of the Langmuir–Finsler space

Since the Jacobi minors method does not accurately allow to find the regions of change of signature by means of vanishing the minors, we shall determine S_i, $i = 1, 2, 3$ by examining the null eigenvalues of the metric tensor g_{ij} (2.6). Moreover, since there exist a distribution of relaxation times, the "timelike" direction, which describes it, is preferred one. Therefore, the Langmuir–Finsler space hosts a metric signature, which we shall find, using eigenvectors.

Taking into account that an eigenvalue λ_3 corresponding to the coordinate φ is always negative and equals to

$$\lambda_3 = -\frac{1}{2}Cr^2,$$

one can find the eigenvalues of the matrix g'_{ij}:

$$g'_{ij} = \begin{pmatrix} 3A\dfrac{\dot{\xi}}{\dot{r}} + B & -\dfrac{3}{2}A\left(\dfrac{\dot{\xi}}{\dot{r}}\right)^2 \\[4mm] -\dfrac{3}{2}A\left(\dfrac{\dot{\xi}}{\dot{r}}\right)^2 & A\left(\dfrac{\dot{\xi}}{\dot{r}}\right)^3 - \dfrac{C}{2} \end{pmatrix}$$

as

$$\lambda_1 = \frac{1}{2}\left(-\sqrt{\frac{1}{4}\left(2Au(u^2 - 3) - C - 2B\right)^2 + 9A^2u^4} + Au(u^2 + 3) + B - C/2\right),$$

$$\lambda_2 = \frac{1}{2}\left(\sqrt{\frac{1}{4}\left(2Au(u^2-3)-C-2B\right)^2 + 9A^2u^4} + Au(u^2+3) + B - C/2\right),$$

where $u = \dot{\xi}/\dot{r}$. The dependencies of λ_1 and λ_2 on $\dot{\xi}/\dot{r}$ are depicted in Fig. 3. The corresponding eigenvectors are

$$\mathbf{v_1} = \frac{3}{2}\frac{Au^2}{(-\lambda_1 + 3Au + B)}\mathbf{e_t} + \mathbf{e_r},$$

$$\mathbf{v_2} = \frac{3}{2}\frac{Au^2}{(-\lambda_2 + 3Au + B)}\mathbf{e_t} + \mathbf{e_r},$$

$$\mathbf{v_3} = \mathbf{e_\varphi}.$$

The eigenvector $\mathbf{v_1}(\mathbf{v_2})$ is then considered as vector directed along the time axis if its absolute value of time component is 100 times the radial component, and converse. According this rule, the signature of the space is not defined in the regions of u where the eigenvectors $\mathbf{v_1}(\mathbf{v_2})$ are substantially of space–time type.

Let the values u for an arbitrary point $\vec{r}_0$ of the monolayer are u_i, $i = 1,2$ for $\lambda_i = 0$ and u_3 at the median point of the region where $\mathbf{v_1}(\mathbf{v_2})$ could not be related with proper time and radial directions. Then, the surfaces S_i, $i = 1,2,3$ which separate the regions with different metric signature are defined by means of $\dot{\xi}/\dot{r} = u_i$, and are the following planes:

$$(2.7) \qquad\qquad r_0\Delta t - u_i(x_0\Delta x + y_0\Delta y) = 0.$$

Table 1 shows the numerically calculated metric signatures of the Finsler space for the eigenvalues and the eigenvectors of g_{ij} depending on A, B and u. Due to the definition (2.3), pieces of the timelike indicatrices related to the metric signature $(-\ -\ -)$ of the Langmuir–Finsler space in Figs. 1a–d are absent. Accordingly, there does exist no stable Langmuir monolayer characterized by such indicatrices. As one can see, the region of physically meaningful values of parameter $\dot{\xi}/\dot{r}$ grows with decreasing values of B, for example, $\dot{\xi}/\dot{r}$ runs over interval $(-\infty;\ -1.3\cdot 10^{16})$ and $(-\infty;\ 3674)$ for $B = 10$ and -10 respectively.
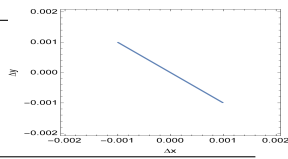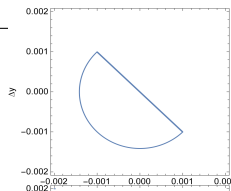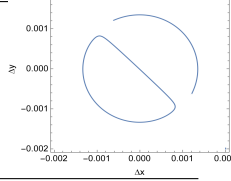
According to the table 1, the motion associated with the indicatrix of types e, ..., h in Figs. 1e–h, is infinite. The motion associated with the indicatrix of types i, ..., k in Figs. 1i–k, is finite accordingly to the table 1. The motion associated with indicatrices of type "i" takes place on the strange attractor of relaxation oscillations [31]. According to the table 1, the regions of finite and infinite motions with indicatrices of type j and k are not overlapping. The sets which separate these regions become thinner and eventually tend to a punctured neighborhood for $\Delta t \to 0$.

We further consider the components $C_{ijk} = \frac{1}{2}\frac{\partial g_{ij}}{\partial y^k}$, $i,j,k \in \overline{1,3}$, of the Cartan tensor, which describes the space torsion. Direct calculations give:

$$C_{111} = \frac{3A}{2}\frac{1}{\dot{r}}, \quad C_{112} = C_{121} = C_{211} = -\frac{3A}{2}\frac{\dot{\xi}}{\dot{r}^2}, \quad C_{122} = C_{212} = C_{221} = \frac{3A}{2}\frac{\dot{\xi}^2}{\dot{r}^3},$$

$$C_{222} = -\frac{3A}{2}\frac{\dot{\xi}^3}{\dot{r}^4}, \quad C_{3ij} = 0, \quad \forall i,j, \in \overline{1,3}.$$

Table 1: Signatures of spacelike indicatrices and types of physical indicatrix projections near reference point in plane XY at different parameters A, B. The indicatrices e, ..., k are depicted Fig. 1e–k.

A, B	Hessian signature $(n_+,\ n_-)$	Metric signature	Range of $\dot{\xi}/\dot{r}$	Indicatrix, its projection
10^{-15}, 10	(0,3)	$(-\ -\ -)$	$(-\infty;\ -1.3 \cdot 10^{16})$	–
	(1, 2)	$(+\ -\ -)$	$(-1.3 \cdot 10^{16};\ 7.9 \cdot 10^6)$	
	(2, 1)	$(+\ +\ -)$	$(7.9 \cdot 10^6;\ +\infty)$	
10^{-5}, 10	(0, 3)	$(-\ -\ -)$	$(-\infty;\ -1.3 \cdot 10^6)$	e
	(1, 2)	$(+\ -\ -)$	$(-1.3 \cdot 10^6;\ 3635)$	
	(1, 2)	$(1, 2)^*$	$(3635;\ 3694)$	
	(2, 1)	$(+\ +\ -)$	$(3694;\ +\infty)$	
10^{-5}, 1	(0, 3)	$(-\ -\ -)$	$(-\infty;\ -1.3 \cdot 10^5)$	f,
	(1, 2)	$(+\ -\ -)$	$(-1.3 \cdot 10^5;\ 3646)$	projection form as for e
	(1, 2)	$(1, 2)^*$	$(3646;\ 3742)$	
	(1, 2)	$(-\ +\ -)$	$(3742;\ 3783)$	
	(2, 1)	$(+\ +\ -)$	$(3783;\ +\infty)$	
10^{-5}, 0.1	(0, 3)	$(-\ -\ -)$	$(-\infty;\ -12380)$	g,
	(1, 2)	$(+\ -\ -)$	$(-12380;\ 3648)$	projection form as for e
	(1, 2)	$(1, 2)^*$	$(3648;\ 3749)$	
	(1, 2)	$(-\ +\ -)$	$(3749;\ 4439)$	
	(2, 1)	$(+\ +\ -)$	$(4439;\ +\infty)$	
10^{-5}, 0.07	(0, 3)	$(-\ -\ -)$	$(-\infty;\ -5685)$	h,
	(1, 2)	$(+\ -\ -)$	$(-5685;\ 3637)$	projection form as for e
	(1, 2)	$(1, 2)^*$	$(3637;\ 3740)$	
	(1, 2)	$(-\ +\ -)$	$(3740;\ 4638)$	
	(2, 1)	$(+\ +\ -)$	$(4638;\ +\infty)$	
10^{-5}, 10^{-15}	(0, 3)	$(-\ -\ -)$	$(-\infty;\ -3.3 \cdot 10^{-11})$	i
	(1, 2)	$(+\ -\ -)$	$(-3.3 \cdot 10^{-11};\ 3637)$	
	(1, 2)	$(1, 2)^*$	$(3637;\ 3737)$	
	(1, 2)	$(-\ +\ -)$	$(3737;\ 5848)$	
	(2, 1)	$(+\ +\ -)$	$(5848;\ +\infty)$	
10^{-5}, -0.1	(0, 3)	$(-\ -\ -)$	$(-\infty;\ 2493)$	j
	(1, 2)	$(+\ -\ -)$	$(2493;\ 3642)$	
	(1, 2)	$(1, 2)^*$	$(3642;\ 3735)$	
	(1, 2)	$(-\ +\ -)$	$(3735;\ 14101)$	
	(2, 1)	$(+\ +\ -)$	$(14101;\ +\infty)$	
10^{-5}, -1	(0, 3)	$(-\ -\ -)$	$(-\infty;\ 3579)$	k,
	(1, 2)	$(+\ -\ -)$	$(3579;\ 3635)$	projection form as for j
	(1, 2)	$(1, 2)^*$	$(3635;\ 3735)$	
	(1, 2)	$(-\ +\ -)$	$(3735;\ 133342)$	
	(2, 1)	$(+\ +\ -)$	$(133342;\ +\infty)$	
10^{-5}, -10	(0, 3)	$(-\ -\ -)$	$(-\infty;\ 3674)$	–
	(1, 2)	$(1, 2)^*$	$(3674;\ 3735)$	
	(1, 2)	$(-\ +\ -)$	$(3735;\ 1.3 \cdot 10^6)$	
	(2, 1)	$(+\ +\ -)$	$(1.3 \cdot 10^6;\ +\infty)$	

We note that * – none of the eigenvectors of $\lambda_{1,\ 2}$ could not be considered as space or time directions.
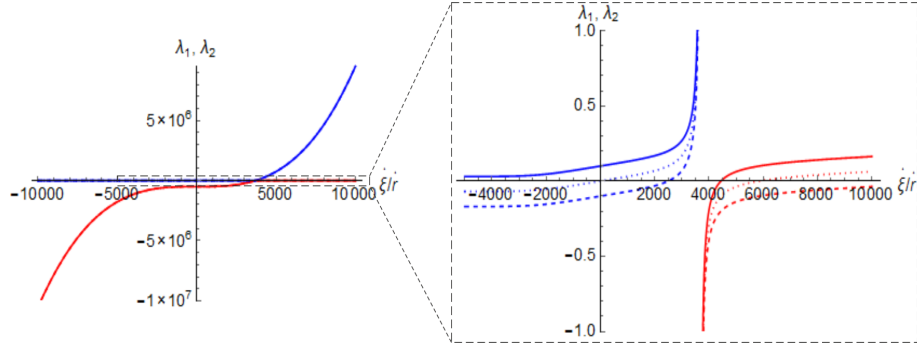
Figure 3: The dependence of the eigenvalues λ_1, λ_2 (blue and red) on $\dot{\xi}/\dot{r}$ at $B = 0.1$ (solid line), 10^{-15} (dotted line) and -0.1 (dashed line). Inset is an expanded fragment of the dependencies.

One gets that the effective components of the Cartan tensor C_{ijk} live on a 2D-plane $\{\dot{r}, \dot{\xi}\}$. Due to the facts that, firstly, the components of the Cartan tensor are determined by the parameter A only and do not depend on B and, secondly, the topological form of indicatrix is determined by values of the parameter B according to the table 1, one concludes that the torsion of space can be conserved during the phase transition and can be very small.

2.3 Nonlinear Barthel connection and mean Berwald curvature

According to [32], we determine the mean Berwald curvature tensor E_{ij}, by the following steps:

$$G^i(y) = \tfrac{1}{4} g^{il}(y) \left\{ 2 \tfrac{\partial g_{jl}}{\partial x^k}(y) - \tfrac{\partial g_{jk}}{\partial x^l}(y) \right\} y^j y^k,$$
$$N^i_j(y) = \tfrac{\partial G^i}{\partial y^j}(y),$$
$$E_{ij} = \tfrac{1}{2} \tfrac{\partial^2}{\partial y^i \partial y^j} \tfrac{\partial G^k}{\partial y^k}$$

where $x^k = \{t, r, \phi\}$, $y^k = \{\dot{\xi}, \dot{r}, \dot{\phi}\}$. The spray coefficients G^i are then:

$$G^1 = \tfrac{A}{4\Delta_2} \left[\tfrac{1}{2} A_t \tfrac{\dot{\xi}^6}{\dot{r}^4} + B_t \tfrac{\dot{\xi}^5}{\dot{r}^3} + \tfrac{1}{2} B_r \tfrac{\dot{\xi}^4}{\dot{r}^2} + \tfrac{3}{2} Cr \tfrac{\dot{\xi}^2 \dot{\varphi}^2}{\dot{r}^2} \right]$$
$$- \tfrac{C}{8\Delta_2} \left[2A_t \tfrac{\dot{\xi}^3}{\dot{r}} + B_t \dot{\xi}^2 + 3A_r \dot{\xi}^2 + 2B_r \dot{\xi}\dot{r} \right],$$
$$G^2 = \tfrac{3}{4} \tfrac{A}{\Delta_2} \left[-\tfrac{1}{2} A_r \tfrac{\dot{\xi}^4}{\dot{r}^2} + \tfrac{1}{2} B_t \tfrac{\dot{\xi}^4}{\dot{r}^2} + Cr \tfrac{\dot{\xi}\dot{\varphi}^2}{\dot{r}} \right]$$
$$- \tfrac{B}{4\Delta_2} \left[A_t \tfrac{\dot{\xi}^4}{\dot{r}^2} + 2A_r \tfrac{\dot{\xi}^3}{\dot{r}} + B_r \dot{\xi}^2 - Cr\dot{\varphi}^2 \right],$$
$$G^3 = \tfrac{1}{r} \dot{r}\dot{\varphi},$$

with

$$A_t = \frac{\partial A}{\partial t}, A_r = \frac{\partial A}{\partial r}, B_t = \frac{\partial B}{\partial t}, B_r = \frac{\partial B}{\partial r}.$$

The components of the nonlinear Barthel connection have the following explicit form:

$$N_1^1 = \frac{A}{4\Delta_2}\left[3A_t\frac{\dot\xi^5}{\dot r^4} + 5B_t\frac{\dot\xi^4}{\dot r^3} + 2B_r\frac{\dot\xi^3}{\dot r^2} + 3Cr\frac{\dot\xi\dot\varphi^2}{\dot r^2}\right] - \frac{C}{4\Delta_2}\left[3A_t\frac{\dot\xi^2}{\dot r} + (B_t + 3A_r)\dot\xi + B_r\dot r\right] - G^1\frac{\dot\Delta_2}{\Delta_2},$$

$$N_2^1 = \frac{A}{4\Delta_2}\left[-2A_t\frac{\dot\xi^6}{\dot r^5} - 3B_t\frac{\dot\xi^5}{\dot r^4} - B_r\frac{\dot\xi^4}{\dot r^3} - 3Cr\frac{\dot\xi^2\dot\varphi^2}{\dot r^3}\right] - \frac{C}{8\Delta_2}\left[-2A_t\frac{\dot\xi^3}{\dot r^2} + B_r\dot\xi\right] + G^1\frac{\dot\Delta_2}{\Delta_2}\frac{\dot\xi}{\dot r},$$

$$N_3^1 = \frac{3AC}{4\Delta_2}r\frac{\dot\xi^2\dot\varphi}{\dot r^2},$$

$$N_1^2 = \frac{3A}{4\Delta_2}\left[Cr\frac{\dot\varphi^2}{\dot r} + 2(B_t - A_r)\frac{\dot\xi^3}{\dot r^2}\right] - \frac{B}{2\Delta_2}\left[2A_t\frac{\dot\xi^3}{\dot r^2} + 3A_r\frac{\dot\xi^2}{\dot r} + B_r\dot\xi\right] - G^2\frac{\dot\Delta_2}{\Delta_2},$$

$$N_2^2 = \frac{3A}{4\Delta_2}\left[(A_r - B_t)\frac{\dot\xi^4}{\dot r^3} - Cr\frac{\dot\xi\dot\varphi^2}{\dot r^2}\right] + \frac{B}{2\Delta_2}\left[A_t\frac{\dot\xi^4}{\dot r^3} + A_r\frac{\dot\xi^3}{\dot r^2}\right] + G^2\frac{\dot\Delta_2}{\Delta_2}\frac{\dot\xi}{\dot r},$$

$$N_3^2 = \frac{3AC}{2\Delta_2}r\frac{\dot\xi\dot\varphi}{\dot r} + \frac{BC}{2\Delta_2}r\dot\varphi, \quad N_1^3 = 0, \quad N_2^3 = \frac{\dot\varphi}{r}, \quad N_3^3 = \frac{\dot r}{r},$$

where

$$\dot\Delta_2 = \left[3A^2\frac{\dot\xi^3}{\dot r^4} + 3AB\frac{\dot\xi^2}{\dot r^3} - \frac{3}{2}AC\frac{1}{\dot r}\right].$$

The mean Berwald curvature tensor components can be found out as second derivatives of the trace of the nonlinear Barthel connection tensor over y^i:

$$(2.8) \qquad\qquad E_{ij} = \frac{1}{2}\frac{\partial^2}{\partial y^i \partial y^j}\left(N_1^1 + N_2^2 + N_3^3\right),$$

where

$$N_1^1 + N_2^2 + N_3^3 = \frac{1}{4\Delta_2}\left[A\frac{\dot\xi^3}{\dot r^2}\left(3A_t\frac{\dot\xi^2}{\dot r^2} + (2B_t + 3A_r)\frac{\dot\xi}{\dot r} + 2B_r\right) + 2B\frac{\dot\xi^3}{\dot r^2}\left(A_t\frac{\dot\xi}{\dot r} + A_r\right)\right.$$

$$(2.9) \qquad\qquad\left. -C\dot r\left(3A_t\frac{\dot\xi^2}{\dot r^2} + (B_t + 3A_r)\frac{\dot\xi}{\dot r} + B_r\right)\right] - \frac{\dot\Delta_2}{\Delta_2}\left[G^1 - G^2\frac{\dot\xi}{\dot r}\right] + \frac{\dot r}{r}.$$

The following analysis of the Berwald curvature is fulfilled by numerical simulation. To this aim, we perform the convolution product of the Berwald curvature tensor with the metric tensor:

$$B_C(x, y) = g^{ij}E_{ij}.$$

Further the Finsler adapted frames for the module of sections of the tangent bundle are constructed to discover features of the 1st-order phase transition model.

The evolution of the monolayer configurations $r(s)$, of their indicatrix projections, and of the Berwald scalar curvature B_C, in dependence on the the compression speed V is shown in Fig. 4. Since the Berwald curvature B_C changes its sign in Fig. 4c, f, i, then in all the considered cases phase transitions of first order occur. However, for
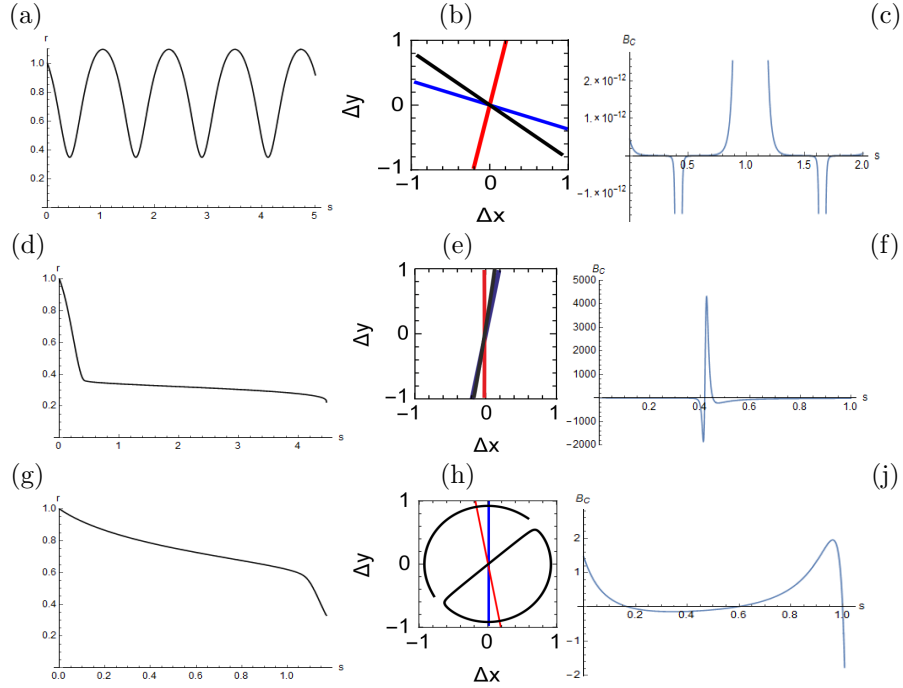
Figure 4: The evolution of the monolayer configurations $r(s)$, of their indicatrix projections, and of the Berwald scalar curvature B_C at different compressed speeds $V=10^{-9}$ (a–c), 0.05 (d–f), 10 (g–j). The evolution parameter s is equal to (b) 0.4 (blue), 1.1 (red), 1.6 (black); (e) 10^{-4} (blue), 1 (red), 4.47 (black); (h)10^{-9} (blue), 0.16 (red), 1.15 (black) respectively.

the case of an isotropic distribution of directions in Fig. 4b the phases periodically lose their stability in the phase transition proceeding at very small compression speed V.

For very small compression speed ($V = 10^{-9}$), the sign of B_C and the configurations $r(s)$ periodically change, as shown in Fig. 4a, c. Meanwhile, the directions of the infinite motion of the particle from Fig. 4b change in an arbitrary way, and effectively produce a set of configurations for the isotropic state, accordingly making the phase transition to be apparently reversible.

At $V = 0.05$ the configuration from Fig. 4d initially exhibits a fast evolution but then evolves slowly, as it usually happens in the 3D phase transition of first order with rapid nucleation and slow nuclei-growth stage. The directions of the movement along configurations in this case are in a narrow range of the velocity values. Since the space of velocities is anisotropic, the configurations at each point of the monolayer are similar to each other. In this way, as result of the phase transition at $V = 0.05$, a crystalline phase emerges.

Opposite to the case $V = 0.05$ with two relaxation times, the monolayer configurations at $V = 10$ from Fig. 4g are characterized by a relaxation-time distribution similar to one for a glass-like state. Meanwhile, all the directions of motion from Fig. 4h are split in two regions: the ones with closed, and with open trajectories.
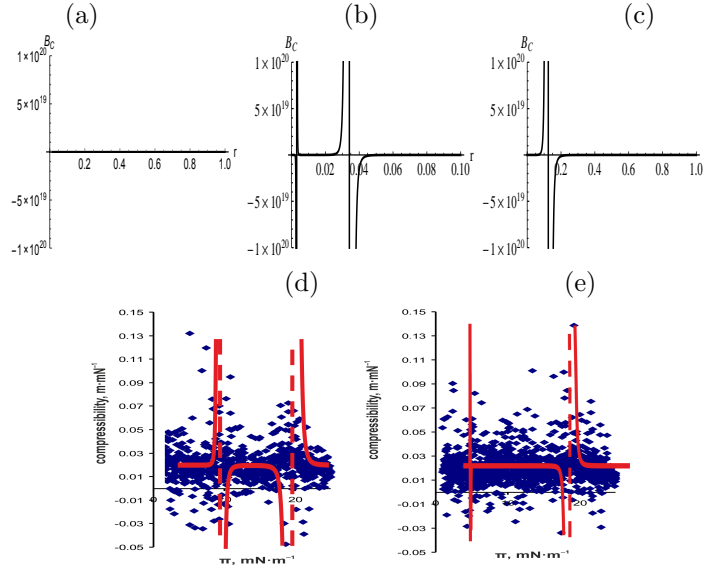
Figure 5: (a–c) The theoretical dependencies of B_C on the radius r at different monolayer compressing rates $V = 10^{-15}$ (a), 2 (b) and 10^{-2} (c). Parameters used: $\dot{r} = 150$, $\dot{\xi} = 20$, $t = 0.01$, $p = 8.9 \times 10^9$. (d–e) The experimental and the fitting theoretical dependence of compressibility κ on r for the monolayer of stearic acid, with the compression speed $V = 6$ mm/min (d) and 5 mm/min (e).

The structures, which are formed in these regions, always coexist, since in the space of velocities there exist punctured locations, which separate the periodic trajectories from the non-closed ones. The periodic trajectories have the form of relaxation oscillations on the strange attractor, as in [31]. Since for very large compression speeds, B_C accepts mostly negative values in the process of phase transition, the particles tend to leave non-closed (open) configurations and transit to the strange attractor. As a result, a fractal glass-like structure of the monolayer is formed.

3   Discussion

The velocities v of the monolayer particles decrease after collisions due to repulsion and, at the same time, the inter-molecular attraction increases the value v. Because of these "random" forces, the compression process has effectively different compression speeds in different regions of the monolayer. Let the configurations $r_1(s)$, $r_2(s)$, ... be geodesic configurations of the regions compressed rapidly or slowly under the action of the random forces.

Theorem 3.1. *The Berwald curvature B_C is determined by the set of all the geodesics r_i, $i = 1, 2, \ldots, N$, for $N \to \infty$.*

Proof. One can rewrite the set $\{r_1, r_2, \ldots, r_N\}$ as $\{r(s_1), r(s_2), \ldots, r(s_N)\}$, $N \to \infty$. Then, the Berwald curvature B_C satisfies the following property:

$B_C(r) = B_C(r(s_i)) \equiv B_C(\{r(s_1), r(s_2), \ldots, r(s_N)\}) = B_C(\{r_1, r_2, \ldots, r_N\})$, for $N \to \infty$. This property proves the claim. $\square$

We shall further study the behavior of the Berwald curvature $B_C(r)$.

We have $B_C = 0$ outside the anomalous phase transition regions, as shown in Fig. 5a–c. Comparing Fig. 4c with Fig. 4f, one can conclude that the width of the anomalous region of phase transition sharply increases for very small compression speed V. The compressibility κ of the monolayer can be determined in terms of the Berwald curvature $B_C(r)$, calculated irrelative of the evolution [33]. According to the calculation performed above, in the case of V large enough, the Berwald curvature $B_C(r)$ of the trajectories behaves anomalously in a very narrow interval of values of the evolution parameter s, while this interval is wide for very small V. Therefore, the sign of the Berwald curvature $B_C(r)$ and, respectively, the sign of κ change twice, as shown in Fig. 5b. Meanwhile, the occurrence of the narrow line from Fig. 5b for relatively large values of V testifies the existence of the isotherm plateau. The wide anomalous regions in Fig. 5b, c, where the distribution of the particle velocities over the directions is isotropic, prove the existence of islands (domains) of both anisotropic and isotropic phases in the monolayer. The experimental dependencies of κ in Fig. 5d, e and in [33, 34] perfectly agree with the theoretically predicted behavior of $B_C(r)$, and with the features of its change for varying V in Fig. 5b,c.

4   Conclusion

We proved that the changes of signature of the model-related pseudo-Finsler space take place during the evolution of the system. These events are associated with the change of the set of configurations with maximal entropy and maximal entropy production entering into the contact statistical manifold of the monolayer. For the monolayer in the phase-transition state there always exist open configurations, when the movement of the particles is infinite. The anisotropy of motion along the configurations is revealed as an isotherm plateau. As well, the Cartan tensor and the nonlinear Barthel connection are determined, which provide a tool to estimate how far is the pseudo-Finsler space from the pseudo-Euclidean one. The Berwald curvature B_C are experimentally exhibited through an anomalous behavior of the compressibility κ of the monolayer. The proposed Finsler–Lagrange theory of 2D first-order phase transitions in Langmuir monolayers is able to foresee three types of structurization in accordance with the experimental dependencies of the compressibility on the compression speed. The developing of such a theory allows to handle a fabrication of nanocomposite LB-structures.

References

[1] I.P. Suzdalev, *Nanotechnology: Physico-Chemistry of Nanoclusters*, Librokom, Moscow 2009.

[2] H.V. Grushevskaya, N.G. Krylova, I.V. Lipnevich, T.I. Orekhovskaja, B.G. Shulitski, *Electrochemical nanobiosensor for real-time detection of gap junction-mediated intercellular communication activity*, Adv. Materials Lett. **8** (2017), 531.

[3] K. B. Blodgett, *Monomolecular films of fatty acids on glass*, J. Amer. Chem. Soc. **56**, 2 (1934), 495–495.

[4] D. K. Schwartz, *Langmuir-Blodgett film structure*, Surface Sci. Rep. **27** (1997), 241–334.

[5] A.S. Egorov, H.V. Krylova, I.V. Lipnevich, B.G. Shulitsky, L.V. Baran, S.V. Gusakova, M.I. Govorov, *A structure of modified multi-walled carbon nanotube clusters on conducting organometallic Langmuir – Blodgett films*, Int. J. Nonlinear Phenomena in Complex Systems, **15** (2012), 121.

[6] N. Aiba, Y. Sasaki, J. Kumaki, *Strong compression rate dependence of phase separation and stereocomplexation between isotactic and syndiotactic poly(methyl methacrylate)s in a Langmuir monolayer observed by atomic force microscopy*, Langmuir **26**, 15 (2010), 12703–12708.

[7] D. Andelman, F. Brochard, C. Knobler and F. Rondelez, *Structure and phase transitions in Langmuir monolayers*, in "Micelles, Membranes, Microemulsions and Monolayers" (Eds: W.M. Gelbart, A. Ben-Shaul, and D. Roux), Springer, Heidelberg 1994, 559–602.

[8] S. Ramos, R. Castillo, *Langmuir monolayers of C_{17}, C_{19}, and C_{21} fatty acids: textures, phase transitions, and localized oscillations*, J. of Chem. Phys. **110**, 14 (1999), 7021–7030.

[9] H.V. Grushevskaya, G.G. Krylov, V.V. Hrushevsky, *Kinetic theory of phase foliation at formation of Langmuir-Blodgett monolayers*, Int. J. Nonlinear Phenomena in Complex Systems **7**, 1 (2004), 17–33.

[10] W. da S. Robazzi, B. J. Mokross, *Influence of interaction energy in fluid-fluid phase transitions on Langmuir monolayers*, Brazilian J. Phys. **36**, 3B (2006), 1013–1016.

[11] L.D. Landau, E.M. Lifshitz, *Statistical Physics, part 1*, In: "Theoretical Physics", vol. 5, PhysMathLit, Moscow 2002; 84–87.

[12] M. Le Bellac, F. Mortessagne, G. G. Batrouni, *Equilibrium and Non-Equilibrium Statistical Thermodynamics*, Cambridge University Press, 2004; 31.

[13] F. Weinhold, *Metric geometry of equilibrium thermodynamics I, II, III, IV*, J. Chem. Phys. **63** (1975); 2479, 2484, 2488, 2496.

[14] F. Weinhold, *Metric geometry of equilibrium thermodynamics V*, J. Chem. Phys. **65** (1976), 558.

[15] G. Ruppeiner, *Thermodynamics: A Riemannian geometric model*, Phys. Rev. A **20** (1979), 1608.

[16] A. Bravetti, F. Nette, *Second order phase transitions and thermodynamic geometry: a general approach*, arXiv: 1208.0399v2 [math-ph] 22 Aug 2012.

[17] H. Quevedo, *Geometrothermodynamics*, J. Math. Phys. **48** (2007), 013506.

[18] K. Binder, *Theory of first-order phase transitions*, Rep. Prog. Phys. **50** (1987), 783–859.

[19] H.V. Grushevskaya, N.G. Krylova, *Effects of Finsler geometry in physics surface phenomena: case of monolayer systems*, H.N.G.P., **1 (15)**, 8 (2011), 128–146.

[20] V. Balan, H.V. Grushevskaya, N.G. Krylova, and M. Neagu, *Multiple-relaxation-time Finsler-Lagrange dynamics in a compressed langmuir monolayer*, Int. J. Nonlinear Phenomena in Complex Systems, **19**, 3 (2016), 223–253.

[21] P. Rashevski, *Polymetric geometry*, In: "Proceedings of Seminar on vector and tensor analysis with its applications into geometry and physics", (Ed.: V.F. Kagan), Vol. 5, State Publishing Company of Technical and Theoretical Literature, Moscow, Leningrad 1941, 21–147.

[22] H. Rund, *Differential Geometry of Finsler Spaces*, Scince Eds., Moscow 1981.

[23] J. Mielczarek, *Signature change in loop quantum cosmology*, In: "Relativity and Gravitation" (Eds.: J. Bicak and T. Ledvinka), Springer Proceedings in Physics, Vol. 157, Springer, Berlin, 2014; 555–562.

[24] A. White, S. Weinfurtner, M. Visser, *Signature change events: a challenge for quantum gravity?* Classical and Quantum Gravity, **27**(4) (2010), 045007.

[25] S. Weinfurtner, A. White, M. Visser, *Trans-Planckian physics and signature change events in Bose gas hydrodynamics*, Phys. Rev. D **76** (2007), 124008.

[26] I.I. Smolyaninov, E.E. Narimano, *Metric signature transitions in optical meta-materials*, Phys. Rev. Lett. **105** (2010), 067402.

[27] U. Gehlert, D. Vollhardt, *Nonequilibrium structures in 1-monopalmitoyl-rac-glycerol monolayers*, Langmuir **13** (1997), 277.

[28] N. Nandi, D. Vollhardt, *Anomalous temperature dependence of domain shape in Langmuir monolayers: Role of dipolar interaction*, J. Phys. Chem. B **108** (2004), 18793.

[29] R. Miron, *Lagrange Geometry*, Mathl. Comput. Modelling **20**, 4/5 (1994), 25–40.

[30] D. Bao, R. L. Bryant, S. Chern, and Z. Shen, *A Sampler of Riemann-Finsler Geometry*, Cambridge University Press, 2004.

[31] G. V. Grushevskaja, A. I. Khmelnitsky, *Sequence of bifurcations in an 'Antigen-antibody' reaction*, J. Molecular Recognition **9**, 5/6 (1996), 570.

[32] Z. Shen, *Lectures in Finsler Geometry*, World Scientific, 2001.

[33] V. Balan, H. Grushevskaya, N. Krylova, *Finsler geometry approach to thermodynamics of first order phase transitions in monolayers*, Diff. Geom. Dyn. Systems **17** (2015), 24.

[34] H.V. Grushevskaya, G.G. Krylov, N.G. Krylova, I.V. Lipnevich, *Modeling of the behavior and statistical analysis of compressibility in the process of Langmuir monolayer structurization*, J. Phys. CS. **643** (2015), 012015.

Authors' addresses:

Vladimir Balan
University Politehnica of Bucharest, Splaiul Independentei 313,
060042 Bucharest, Romania, E-mail: vladimir.balan@upb.ro

Halina V. Grushevskaya, Nina G. Krylova, George G. Krylov, and Ihor V. Lipnevich
Faculty of Physics, Belarusan State University, 4 Nezavisimosti Ave.,
220030 Minsk, The Republic of Belarus.
E-mail: grushevskaja@bsu.by , nina-kr@tut.by , krylov@bsu.by , lipnevich@bsu.by